Inorganic Chemistry

Article

pubs.acs.org/IC

Theoretical and Experimental Study of the Crystal Structures, Lattice Vibrations, and Band Structures of Monazite-Type $PbCrO_4$, $PbSeO_4$, $SrCrO_4$, and $SrSeO_4$

Daniel Errandonea,*[,†] Alfonso Muñoz,[‡] Placida Rodríguez-Hernández,[‡] John E. Proctor,[§] Fernando Sapiña,[⊥] and Marco Bettinelli[∥]

[†]Departamento de Física Aplicada, ICMUV, MALTA Consolider Team, Edificio de Investigación, Universidad de Valencia, C. Dr. Moliner 50, 46100 Burjassot, Spain

[‡]Departamento Física, Malta Consolider Team, and Instituto de Materiales y Nanotecnología, Universidad de La Laguna, 38206 La Laguna, Tenerife, Spain

[§]Joule Physics Laboratory, University of Salford, Manchester M5 4WT, U.K.

[⊥]Institut de Ciencia dels Materials (ICMUV), Universitat de Valencia, C/Catedrático José Beltrán 2, 46890 Paterna, Spain

[∥]Luminescent Materials Laboratory, Department of Biotechnology, University of Verona and INSTM, UdR Verona, Strada Le Gracie 15, 37134 Verona, Italy

ABSTRACT: The crystal structures, lattice vibrations, and electronic band structures of $PbCrO_4$, $PbSeO_4$, $SrCrO_4$, and $SrSeO_4$ were studied by ab initio calculations, Raman spectroscopy, X-ray diffraction, and optical-absorption measurements. Calculations properly describe the crystal structures of the four compounds, which are isomorphic to the monazite structure and were confirmed by X-ray diffraction. Information is also obtained on the Raman- and IR-active phonons, with all of the vibrational modes assigned. In addition, the band structures and electronic densities of states of the four compounds were determined. All are indirect-gap semiconductors. In particular, chromates are found to have band gaps smaller than 2.5 eV and selenates higher than 4.3 eV. In the chromates (selenates), the upper part of the valence band is dominated by O 2p states and the lower part of the conduction band is composed primarily of electronic states associated with the Cr 3d and O 2p (Se 4s and O 2p) states. Calculations also show that the band gap of $PbCrO_4$ ($PbSeO_4$) is smaller than the band gap of $SrCrO_4$ ($SrSeO_4$). This phenomenon is caused by Pb states, which, to some extent, also contribute to the top of the valence band and the bottom of the conduction band. The agreement between experiments and calculations is quite good; however, the band gaps are underestimated by calculations, with the exception of the bang gap of $SrCrO_4$, for which theory and calculations agree. Calculations also provide predictions of the bulk modulus of the studied compounds.

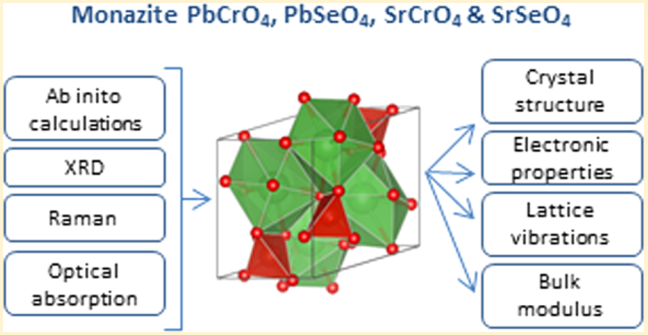

1. INTRODUCTION

Recently, there has been a large amount of interest in the study of monazite-type structured oxides. These compounds have importance in areas such as earth, planetary, and materials sciences.[1−12] Because of their relevance, most of the studies have been focused on monazite-type structured phosphates. Among other oxides, only $LaVO_4$, $PbCrO_4$, and $CaSeO_4$ have been thoroughly studied.[1,2,6,7,12] For other compounds, like $SrCrO_4$, $PbSeO_4$, and $SrSeO_4$, their crystal structures have been experimentally determined, but few of their Raman-active modes have been measured. In the case of $SrCrO_4$, attempts have been made to determine the electronic band gap, but values ranging from 2.4 to 2.9 eV can be found in the literature.[13−15]

Ab initio calculation has shown to be an accurate method to study the physical and chemical properties of $CaSeO_4$ and compounds related to the monazites.[1] Usually, these quantum-mechanical calculations provide an accurate description of these kinds of oxides, allowing both a better understanding of the experimental results and making accurate predictions. On the basis of this and the facts described above, we consider it timely to perform a theoretical study of $PbCrO_4$, $PbSeO_4$, $SrCrO_4$, and $SrSeO_4$. X-ray diffraction (XRD), Raman spectroscopy, and optical-absorption experiments were also carried out. The combinations of calculations and experiments have allowed us to systematically study the structural, lattice-dynamics, and electronics properties of the four above-mentioned compounds, making considerable progress in their understanding. The knowledge of the studied properties for the chromates is important for their technological applications.[16−18] The inclusion of selenates in the study was done with the aim of better understanding the physical properties of the whole family

Received: May 19, 2015
Published: July 10, 2015

DOI: 10.1021/acs.inorgchem.5b01135
Inorg. Chem. 2015, 54, 7524−7535

of monazite-type oxides. The reported results will be compared with the literature.

The paper is organized as follows: In the next section, we give a detailed description of the experimental techniques. The computational details are presented in section 3. The crystal structures of the four compounds are described together with the vibrational and electronic properties in section 4. Finally, we summarize the results of this work in section 5.

2. EXPERIMENTAL METHODS

$SrCrO_4$ in powder form was prepared by precipitation by adding 50 mL of a 1 M $Sr(NO_3)_2$ solution to 50 mL of a 1 M K_2CrO_4 solution. Single crystals were grown using a ternary flux system composed of NaCl, KCl, and CsCl, as described by Schenker et al.[19] The weight composition of the mixture was NaCl (24.8%), KCl (26.4%), CsCl (41.3%), and $SrCrO_4$ (7.5%). The starting reagents were mixed, placed in a platinum crucible with a tight-fitting lid, and kept for 12 h at 620 °C in a horizontal furnace under an air atmosphere. The melt was slowly cooled first to 530 °C with a temperature gradient of −1.5 °C/h, then to 450 °C at −2 °C/h, and finally to room temperature at −50 °C/h. The crystals were separated by careful dissolution of the flux in deionized water. Yellow single crystals of about 1 × 1 × 1 mm^3 were obtained.

The $PbCrO_4$ crystals used for the experiments reported here were obtained from natural crocoite minerals provided by Excalibur Mineral Company. Electron microprobe analysis found that the only impurity present at a detectable level was iron (0.06%). Crystals were translucent with a red-orange color, and their dimensions were about 10 × 1 × 1 mm^3.

Powder $SrSeO_4$ and $PbSeO_4$ were prepared by precipitation from aqueous solutions of strontium chloride and sodium selenate, and lead acetate and sodium selenate, adapting the synthesis described by Pistorius and Pistorius.[20] The strontium chloride solution was prepared by the addition of a 2 M HCl solution (13.6 mL) to a strontium carbonate suspension in water (2.00 g of $SrCO_3$ in 11.4 mL of H_2O). The lead acetate solution was prepared by dissolving the reagent in water (5.14 g of in 25 mL of H_2O). The sodium selenate solutions were prepared by the addition of water (7.9 mL) and a 2 M sodium hydroxide solution (13.6 mL) to a commercial 40 wt % solution of selenic acid (4.91 g). The selenate solution was then added dropwise to the strontium and lead solutions, and precipitation occurs. In both cases, the pH of the resulting suspensions was adjusted to be 7−8. The suspensions were then heated at 80 °C for 2 h. The solids were separated by filtration, washed with cold water, and dried in air.

It was confirmed by powder XRD using Cu Kα radiation that the $PbCrO_4$, $SrCrO_4$, and $SrSeO_4$ samples are single-phased and present the monazite-type structure (space group $P2_1/n$). Their unit-cell parameters are in very good accordance with those determined by Effenberg and Pertlik from single-crystal XRD experiments.[21] On the other hand, the XRD pattern of $PbSeO_4$ corresponds to a mixture of a majority phase, which can be assigned to the monazite-type structure,[21] and a minority phase, which can be assigned to the β-$PbSeO_4$ orthorhombic barite-type structure (space group *Pnma*).[22] The description of the orthorhombic structure and its relationship with the monazite structure have been described in the literature.[23] There is a group−subgroup relationship between barite and monazite, and the main difference between them is given by the orientation of the CrO_4 tetrahedra.[23] A more detailed description of the barite-type phases of $PbSeO_4$ and $PbCrO_4$ is beyond the scope of this work and can be found in the work by Knight.[23] In spite of the phase coexistence of the synthesized $PbSeO_4$ powder, after dividing it into small fractions, we have been able to find portions of it in which XRD only detected the monazite-type phase. These samples were used for the experiments described here.

Raman experiments were performed for $SrCrO_4$, $PbSeO_4$, and $SrSeO_4$ in the backscattering geometry using a 532 nm laser with a power of less than 20 mW to avoid sample heating. Laser power reduction to 5 mW does not produce changes other than an intensity reduction in the Raman spectra, confirming that sample heating did not affect our experiments. The scattered light was analyzed with a single spectrograph (Shamrock 303i) equipped with an edge filter and an air-cooled multichannel charge-coupled-device detector (iDus 420). The spectral resolution was better than 2 cm^{-1}. For $PbCrO_4$, Raman experiments were carried out by our group in the backscattering geometry using a Horiba Yvon Jobin LabRam spectrometer and were previously published.[17] The results of those experiments have been included here for comparison with ab initio calculations and with the experiments performed in the other three compounds. For $PbCrO_4$, a 632 nm laser was used in the Raman experiments because of the high absorption of $PbCrO_4$ at 532 nm.

In the optical-absorption studies, we used for $PbCrO_4$ and $SrCrO_4$ 20-μm-thick parallel face crystals, which were cleaved from the larger single crystals that we described above. For $PbSeO_4$ and $SrSeO_4$, 20-μm-thick polycrystalline platelets were employed. The platelets were obtained by compressing a powder sample to 1 GPa using a large-volume press equipped with Bridgman anvils.[24] Optical-absorption measurements in the ultraviolet−visible−near-infrared (UV−vis−NIR) have been carried out by making use of both deuterium and halogen lamps integrated in the DH-2000 light-source from Ocean Optics. Light was collimated and focused on the samples by a confocal system consisting of a pair of Cassegrain reflecting objectives (15×). Transmittance of the samples was measured using the sample in/sample out method and detected with an Ocean Optics USB2000 UV−vis−NIR spectrometer.[25−27] From it, we determined the absorption-coefficient spectrum and the energy of the fundamental band gap (E_g).

3. OVERVIEW OF THE CALCULATIONS

The ab initio simulations were performed with the Vienna Ab-initio Simulation Package (*VASP*)[28] program in the framework of density functional theory (DFT).[29] The atomic species were described with projected-augmented-wave pseudopotentials.[30] The exchange-correlation energy was taken in the generalized gradient approximation with the PBEsol prescription.[31] Because of the presence of oxygen, a cutoff energy of 520 eV was used in order to obtain accurate results when calculating the valence electronic wave functions expanded in a plane-wave basis set. A dense Monkhorst−Pack[32] special *k*-points grid was used for the Brillouin zone (BZ) integrations in all of our simulations. The *k*-points sampling and cutoff energy employed ensure a high convergence, better than 1 meV per formula unit, in the total energy. The optimized lattice external and internal parameters at different selected volumes were obtained for each compound by fully relaxing all of the internal atom positions and external lattice constants until the forces on the atoms were lower than 0.006 eV/Å and the stress tensor was diagonal, with differences smaller than 0.1 GPa (hydrostatic conditions). Our calculations provided a set of accurate energy (E), volume (V), and pressure (P) data for each compound, from which we obtained the crystal structure at ambient conditions and the $P-V$ equation of state (EOS) for the studied compounds. The band structure and electronic density of states (DOS) are also calculated.

The direct method (direct force-constant approach)[33] was employed to study the lattice vibrations. The lattice-dynamic simulations of phonon modes were performed at the zone center (Γ point) of the BZ. The construction of the dynamical matrix at the Γ point required performing highly accurate calculations of the forces on the atoms when fixed small displacements from the equilibrium configuration of the atoms are considered. The number of needed independent displacements was reduced by using the crystal symmetry. Diagonalization of this matrix provided the frequencies of the modes, their symmetry, and their polarization vectors as well as the

DOI: 10.1021/acs.inorgchem.5b01135
Inorg. Chem. 2015, 54, 7524−7535

Table 1. Unit-Cell Parameters and Volume Calculated for $PbCrO_4$, $PbSeO_4$, $SrCrO_4$, and $SrSeO_4$ Using DFT[a]

	$PbCrO_4$			$PbSeO_4$			$SrCrO_4$			$SrSeO_4$		
	DFT	expt	expt[21]	DFT	expt	expt[21]	DFT	expt	expt[21]	DFT	expt	expt[21]
a (Å)	7.1167	7.098(7)	7.127(2)	7.1780	7.151(7)	7.154(4)	7.0846	7.071(7)	7.065(4)	7.1106	7.102(7)	7.101(2)
b (Å)	7.4145	7.410(7)	7.438(2)	7.4200	7.403(7)	7.407(4)	7.3843	7.379(7)	7.375(4)	7.3468	7.349(7)	7.340(2)
c (Å)	6.7566	6.779(7)	6.799(2)	6.9500	6.950(7)	6.954(4)	6.6972	6.747(7)	6.741(4)	6.8547	6.856(7)	6.874(2)
β (deg)	102.55	102.4(2)	102.43(2)	103.46	103.2(2)	103.14(4)	103.27	103.1(2)	103.08(4)	103.63	103.5(2)	103.48(2)
V (Å^3)	348.006	348.2(9)	351.9(3)	359.996	358.2(9)	358.8(5)	341.009	342.9(9)	342.1(5)	348.007	349.3(9)	348.4(3)

[a]Experimental parameters from this work and the literature[21] are also included for comparison.

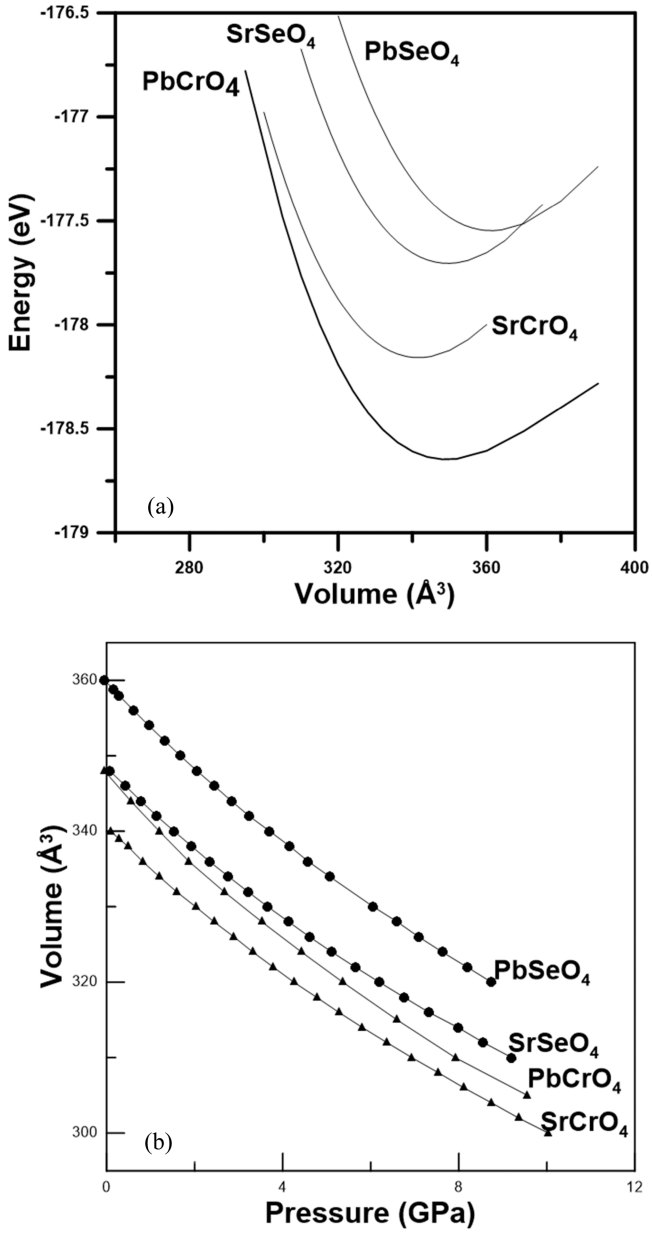

Figure 1. (a) Energy−volume curves calculated for $PbCrO_4$, $SrCrO_4$, $PbSeO_4$, and $SrSeO_4$. In order to facilitate comparison, the energy curve of $SeSeO_4$ was shifted down by −43 eV, the energy curve of $PbSeO_4$ was shifted down by −23 eV, and the energy curve of $PbCrO_4$ was shifted down by −10 eV. (b) Unit-cell volume versus pressure for the four studied compounds.

irreducible representations and the character of the phonon modes at the Γ point. Temperature effects and zero-point energy have been included with the vibrational free energy calculated within the quasi-harmonic approximation.[34−37] Finally, the supercell method was used to obtain the phonon dispersion, phonon density of states (PDOS), and projected DOS.

4. RESULTS

We will start describing the results of the XRD experiments. The structures of these compounds were accurately determined 3 decades ago by Effenberg and Pertlik,[21] and we have confirmed that our samples have the monazite-type structure and determined the unit-cell parameters. These parameters are

DOI: 10.1021/acs.inorgchem.5b01135
Inorg. Chem. 2015, 54, 7524−7535

given in Table 1. They agree within 0.5% with those reported in the literature.[21]

We will now compare our structural calculations with the experimental results. We have made total energy calculations to determine the crystal structures of $PbCrO_4$, $PbSeO_4$, $SrCrO_4$, and $SrSeO_4$. The equilibrium unit-cell parameters were calculated by minimizing the crystal total energy obtained for different volumes. The atomic positions at the equilibrium volume were also calculated. Figure 1a shows the energy−volume curves for the four compounds. For the equilibrium volume, the calculated vibrational free energies in the quasi-harmonic approximation, at 300 K and including the zero-point energy, are 60.7, 78.5, 115.9, and 135.4 meV/pfu (per formula unit) for $PbSeO_4$, $PbCrO_4$, $SrSeO_4$, and $SrCrO_4$, respectively. The calculated unit-cell parameters are given in Table 1. The agreement with the experimental data is excellent. In Table 2,

Table 2. Calculated Atomic Positions for Monazite-Type $PbCrO_4$, $PbSeO_4$, $SrCrO_4$, and $SrSeO_4$[a]

	$PbCrO_4$		
Pb	0.2194 [0.22130]	0.1426 [0.14545]	0.4000 [0.39692]
Cr	0.2012 [0.20107]	0.1654 [0.16364]	0.8824 [0.88184]
O_1	0.2509 [0.2538]	0.0085 [0.0042]	0.0607 [0.0574]
O_2	0.1244 [0.1245]	0.3464 [0.3425]	−0.0146 [−0.0110]
O_3	0.0321 [0.0295]	0.0982 [0.0999]	0.6852 [0.6858]
O_4	0.3882 [0.3859]	0.2137 [0.2141]	0.7847 [0.7819]
	$PbSeO_4$		
Pb	0.2157 [0.21598]	0.1479 [0.14932]	0.4053 [0.40191]
Se	0.1948 [0.19595]	0.1644 [0.16362]	0.8823 [0.88195]
O_1	0.2365 [0.2397]	0.0029 [0.0057]	0.0526 [0.0490]
O_2	0.1163 [0.1196]	0.3440 [0.3396]	−0.0139 [−0.0142]
O_3	0.0255 [0.0252]	0.1090 [0.1102]	0.6796 [0.6851]
O_4	0.3826 [0.3806]	0.2081 [0.2083]	0.7871 [0.7881]
	$SrCrO_4$		
Sr	0.2269 [0.22813]	0.1574 [0.15869]	0.3980 [0.39806]
Cr	0.1974 [0.19769]	0.1651 [0.16487]	0.8860 [0.88691]
O_1	0.2583 [0.2584]	0.0033 [0.0055]	0.0597 [0.0562]
O_2	0.1188 [0.1201]	0.3393 [0.3373]	0.0018 [0.0024]
O_3	0.0231 [0.0256]	0.1002 [0.1012]	0.6917 [0.6981]
O_4	0.3798 [0.3776]	0.2214 [0.2179]	0.7848 [0.7881]
	$SrSeO_4$		
Sr	0.2199 [0.22082]	0.1561 [0.15773]	0.4005 [0.39876]
Se	0.1931 [0.19364]	0.1647 [0.16510]	0.8857 [0.88588]
O_1	0.2467 [0.2484]	0.0029 [0.0052]	0.0592 [0.0552]
O_2	0.1125 [0.1154]	0.3392 [0.3375]	0.0000 [−0.0004]
O_3	0.0178 [0.0192]	0.1049 [0.1094]	0.6868 [0.6935]
O_4	0.3774 [0.3752]	0.2154 [0.2167]	0.7859 [0.7872]

[a]All atoms are at 4e Wyckoff positions. The experimental positions[21] are also included in square brackets for comparison.

we present the calculated atomic positions and compare them with those obtained from single-crystal XRD.[21] The agreement between the calculations and experimental results is again excellent. Both facts indicate that DFT calculations accurately describe the crystal structures of the four studied compounds, suggesting that DFT could be a powerful tool to calculate other physical properties of $PbCrO_4$, $PbSeO_4$, $SrCrO_4$, and $SrSeO_4$. In particular, from the energy−volume curves shown in Figure 1a, we obtained the pressure dependence of the unit-cell volume. The results we obtained are shown in Figure 1b. It can be seen that the four compounds have similar compressibilities, with $PbCrO_4$ being the most compressible compound among them. We also fitted the energy−volume curves with a Birch−Murnaghan third-order EOS[38] to determine the bulk modulus and its pressure derivative, two important parameters that characterized the behavior of the materials under compression. These parameters are given in Table 3. For $PbCrO_4$, the

Table 3. Unit-Cell Volume (V_0), Bulk Modulus (B_0), and Its Pressure Derivative (B'_0) Determined Using a Third-Order Birch−Murnaghan EOS To Fit the DFT Results of Figure 1

	V_0 (Å^3)	B_0 (GPa)	B_0'
$PbCrO_4$	348	51.89	4.92
$PbSeO_4$	360	56.75	4.56
$SrCrO_4$	341	58.70	4.58
$SrSeO_4$	348	57.83	5.08

theoretical bulk modulus (51.89 GPa) is comparable with the experimental value (56 ± 1 GPa),[2] which was determined with a second-order Birch−Murnaghan EOS. In our case, if the second-order EOS is used in the fitting of the energy−volume curves, the bulk modulus is 53.84 GPa. For the other three compounds, there are no previous results to compare them with. According to our calculations, $PbCrO_4$ ($PbSeO_4$) is more compressible than $SrCrO_4$ ($SrSeO_4$), which is consistent with the behavior observed when $PbMoO_4$ ($PbWO_4$)[39,40] is compared with $SrMoO_4$ ($SrWO_4$).[41,42]

We will now discuss the vibrational properties of the studied materials. From factor group analysis, it can be established that the monazite structure presents 36 Raman-active phonons ($\Gamma = 18B_g + 18A_g$), 33 IR-active phonons ($\Gamma = 16B_u + 17A_u$), and three acoustic phonons ($\Gamma = 2B_u + 1A_u$) at the zone center. The Raman- and IR-active modes have been reported earlier for

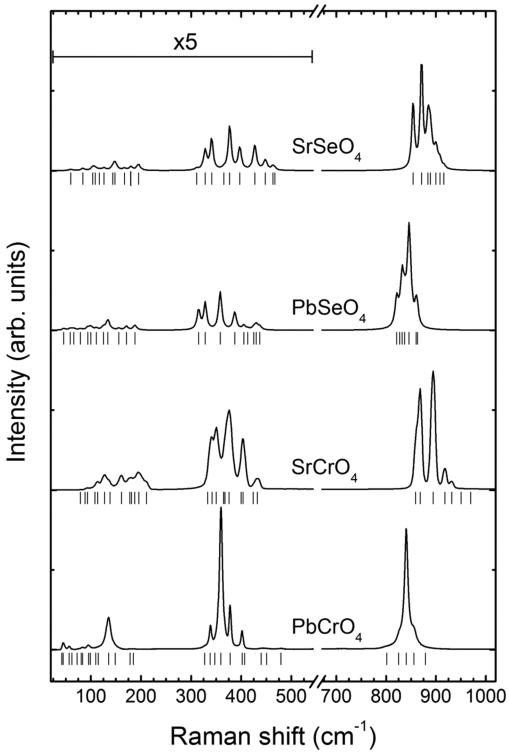

Figure 2. Raman spectra of the four studied compounds. The low-frequency region is magnified (5×) to better show the modes of this region, which are the least intense modes.

DOI: 10.1021/acs.inorgchem.5b01135
Inorg. Chem. 2015, 54, 7524−7535

Table 4. Experimental (expt) and Calculated (theory) Raman Modes of All Monazite Compounds (cm^{-1}) Including Mode Assignment

$PbSeO_4$			$SrSeO_4$			$SrCrO_4$			$PbCrO_4$		
mode	theory	expt	mode	theory	expt	mode	theory	expt	mode	theory	expt
A_g	46.70	46	B_g	60.04	60	B_g	58.37		A_g	43.83	42
B_g	47.40		A_g	69.25		A_g	64.81		B_g	44.60	45
A_g	48.93		A_g	76.39		A_g	76.62	79	A_g	49.83	
B_g	58.41	59	B_g	84.59	84	A_g	91.66	89	B_g	52.40	57
A_g	61.31		A_g	93.40		B_g	92.16	94	A_g	54.77	62
B_g	66.25	66	B_g	104.47	104	B_g	106.61	108	B_g	61.98	73
A_g	79.09	79	B_g	109.28	109	A_g	109.68		B_g	81.80	81
B_g	81.59		A_g	112.34		B_g	114.38	114	A_g	85.13	83
A_g	94.80		B_g	117.62	117	B_g	119.42		A_g	99.87	95
A_g	99.34	100	A_g	126.42	126	A_g	122.69	127	A_g	104.41	99
B_g	107.34		A_g	127.52		A_g	130.29	138	B_g	110.41	110
B_g	108.51	111	B_g	144.30	144	B_g	155.04		B_g	121.75	116
B_g	125.69	125	A_g	148.74	148	A_g	158.74	161	A_g	137.56	136
A_g	129.96		B_g	167.08	167	B_g	174.72	177	B_g	145.27	149
B_g	135.20	134	B_g	168.75		B_g	184.36	181	B_g	146.77	
A_g	155.11	156	A_g	188.40	180	B_g	192.13	187	A_g	158.08	178
B_g	182.56	171	B_g	197.14	195	A_g	192.40	196	B_g	184.43	185
A_g	191.53	188	A_g	204.84		A_g	197.40	211	A_g	185.00	
B_g	285.40		B_g	295.44	311	B_g	333.60	333	B_g	321.76	327
A_g	297.17	315	A_g	308.91	328	A_g	344.17	342	A_g	335.13	338
A_g	327.90	328	A_g	347.31	341	B_g	349.04	350	B_g	346.51	347
B_g	353.24	358	A_g	365.22	365	A_g	359.88	364	A_g	346.67	359
A_g	356.05	387	B_g	376.69	377	A_g	367.12	367	A_g	353.71	378
A_g	371.69	405	A_g	391.74	397	B_g	389.44	376	B_g	369.96	402
B_g	379.50	413	B_g	391.74	427	A_g	391.84	398	A_g	367.00	407
B_g	389.44	425	B_g	411.72	448	B_g	399.24	403	B_g	375.39	440
A_g	399.64	430	A_g	434.30	463	B_g	423.16	424	B_g	393.97	451
B_g	408.35	437	B_g	440.20	467	A_g	429.10	432	A_g	394.21	479
A_g	774.34		A_g	814.50		B_g	901.39	859	A_g	866.83	801
A_g	791.28	821	B_g	821.04	854	A_g	904.16	868	A_g	877.64	825
B_g	791.85	827	A_g	830.14	871	A_g	910.20		B_g	879.78	
A_g	808.23	832	A_g	838.45	884	A_g	933.91	894	A_g	886.35	840
B_g	808.29	837	B_g	845.89	889	B_g	938.72	918	B_g	894.32	
B_g	809.79	846	A_g	858.76	900	A_g	941.05	932	A_g	906.46	856
A_g	821.44	860	B_g	866.27	908	B_g	959.73	951	B_g	914.63	879
B_g	826.41	863	B_g	870.40	916	B_g	975.61	970	B_g	922.74	

$PbCrO_4$, $PbSeO_4$, $SrCrO_4$, and $SrSeO_4$.[43,44] However, less than half of the expected Raman and IR modes have been measured.[43,44] In contrast, for the case of $PbCrO_4$, our recent Raman measurements,[17] performed using state-of-the-art techniques, found 30 Raman-active modes. Here we report new Raman experiments for $PbSeO_4$, $SrCrO_4$, and $SrSeO_4$. These results, together with those we previously reported for $PbCrO_4$, will be compared here with previous studies[43,44] and our ab initio calculations. Figure 2 shows the Raman spectra of the four compounds. All of the studied compounds do not have Raman-active modes from 500 to 800 cm^{-1}. The Raman modes in the low-wavenumber region are weaker than the modes in the high-wavenumber region. For these reasons, we introduced in the plot a break in the horizontal axis and magnified 5 times the Raman spectra in the low-wavenumber region to facilitate identification of the Raman modes on it. The first conclusion we obtained from the figure is that the four compounds have a similar overall mode distribution. Ticks in the figure show the identified Raman modes. A total of 30 modes have been detected for $PbCrO_4$ and $SrCrO_4$ and 28 modes for $PbSeO_4$ and $SrSeO_4$. A Lorentzian multipeak fitting analysis was used to identify partially overlapping peaks.[45] The wavenumbers determined for the observed Raman modes are summarized in Table 4. In those cases, a comparison with the literature[43,44] is possible and the agreement is quite good. Table 4 also gives the theoretically calculated wavenumbers. Calculations also allowed us to make a mode assignment, which is given in the table. It can be seen that the agreement between theory and experiments is excellent in the low-frequency region (below 205 cm^{-1}). For the rest of the Raman modes, theory and experiments agree within 10%. This small discrepancy between the DFT calculations and experiments has previously been observed in related compounds.[9,46] In particular, in the high-frequency region (above 750 cm^{-1}), the wavenumbers are underestimated by calculations in selenates and overestimated in chromates; see Table 4.

The crystal structure of monazite has been broadly discussed in the literature.[47] In our case, it can be viewed as being

DOI: 10.1021/acs.inorgchem.5b01135
Inorg. Chem. 2015, 54, 7524−7535

Table 5. Experimental (expt)[32,33] and Calculated (theory) IR Modes of All Monazite Compounds (in cm^{-1}) Including Mode Assignment

$PbSeO_4$			$SrSeO_4$			$SrCrO_4$			$PbCrO_4$		
mode	theory	expt	mode	theory	expt	mode	theory	expt	mode	theory	expt
A_u	50.80		A_u	75.89		A_u	74.48		A_u	48.53	
B_u	56.37		B_u	78.29		B_u	82.19		A_u	55.77	
A_u	58.81		A_u	98.63		A_u	100.84		B_u	55.84	
B_u	74.85		B_u	107.81		A_u	102.97		A_u	75.52	
A_u	81.36		A_u	111.01		B_u	114.75		B_u	77.89	
A_u	87.13		B_u	119.18		B_u	129.86		B_u	90.33	
B_u	93.23		A_u	129.49		A_u	131.69		A_u	99.90	
B_u	103.07		A_u	143.07		A_u	140.50		A_u	114.91	
A_u	106.47		B_u	148.70		B_u	146.30		B_u	117.21	
B_u	108.44		B_u	149.90		B_u	152.71		B_u	121.18	
A_u	133.09		A_u	172.39		A_u	159.98		A_u	132.66	
B_u	145.33		A_u	176.82		B_u	185.39		A_u	154.11	
A_u	154.87		B_u	180.02		A_u	188.63		B_u	157.18	
A_u	170.98		A_u	194.33		A_u	200.64		A_u	167.98	
B_u	178.62		B_u	208.44		B_u	210.78		B_u	177.46	
A_u	276.59		B_u	288.83		B_u	324.89		B_u	314.22	
B_u	279.93		A_u	290.27		A_u	331.90		A_u	318.92	
A_u	332.06		A_u	343.40		A_u	339.13		A_u	335.37	
B_u	343.90		B_u	365.22		B_u	367.92	350	B_u	344.37	
A_u	359.72		A_u	376.83		A_u	375.89		A_u	351.38	
B_u	363.75	366	B_u	380.43	381	A_u	379.16		A_u	362.42	
A_u	380.23	372	A_u	399.84	396	B_u	383.30		B_u	371.22	
B_u	382.63	394	B_u	400.38	414	B_u	397.54		B_u	379.33	
B_u	396.84	415	B_u	421.26	425	B_u	423.86	410	B_u	390.37	397
A_u	407.11	427	A_u	443.87	447	A_u	441.91	431	A_u	415.45	
B_u	769.53		B_u	806.02		B_u	888.11	845	B_u	860.13	833
A_u	773.87		A_u	806.06		A_u	892.32	855	A_u	871.00	858
B_u	785.18		B_u	829.31		A_u	914.57	875	B_u	876.04	
A_u	790.18		A_u	829.37	844	B_u	916.93	887	A_u	878.74	
A_u	807.89		B_u	841.92	867	B_u	934.55	912	B_u	885.25	
B_u	807.89	820	A_u	846.35	884	A_u	946.45	927	A_u	893.75	
B_u	831.31	827	B_u	871.90	904	B_u	960.03		B_u	924.81	905
A_u	835.98	857	A_u	877.61	919	A_u	969.44		A_u	929.18	

composed of [001] chains formed of alternating polyhedral SrO_9 (PbO_9) and SeO_4 (CrO_4) tetrahedral units. Therefore, to a good approximation, the monazite structure can be considered as composed of two alternating sublattices separately containing the Sr (Pb) and SeO_4 (CrO_4) ions. As a consequence, the vibrational spectra of monazites have been interpreted in terms of internal modes associated with the SeO_4 (CrO_4) tetrahedron,[48] in which the center of mass of the SeO_4 (CrO_4) units does not move, or external modes, when they involve movements of both the Sr (Pb) and SeO_4 (CrO_4) ions. The external modes can be divided into translational- and rotational-like modes, and the internal modes can be classified as bending and stretching modes. In general, the external modes occur at low wavenumber.[48] In addition, the internal stretching modes are the most intense modes and occur at the highest frequencies.

According to our calculations, we tentatively assigned the external and internal modes of the four studied compounds. They are separated by extra rows of space in Table 4. The modes on the top of the table are the external modes (wavenumbers between 0 and 210 cm^{-1}). The modes in the center of the table are the internal bending modes (wavenumbers between 300 and 475 cm^{-1}), and the modes in the bottom of the table are the internal stretching modes (wavenumbers between 750 and 1000 cm^{-1}). As expected, the last modes are the most intense modes in our experiments; see Figure 2. In particular, the most intense mode is the symmetric stretching A_g mode,[43,44,48] usually named as $\nu_1(A_g)$. In our experiments, the most intense modes are located at 840 cm^{-1} in $PbCrO_4$, 846 cm^{-1} in $PbSeO_4$, 868−894 cm^{-1} in $SrCrO_4$, and 871 cm^{-1} in $SrSeO_4$, suggesting that these are the symmetric stretching A_g modes of the four compounds. Previously, Scheuermann et al.[43,44] tentatively made the same mode assignment in $PbCrO_4$ and $PbSeO_4$. On the other hand, these authors proposed the mode at 860−868 cm^{-1} in $SrCrO_4$ and 854−870 cm^{-1} in $SrSeO_4$ as the symmetric stretching A_g mode. In $SrSeO_4$, the second mode agrees with our suggestion for this. In $SrCrO_4$, the mode at 868 cm^{-1} proposed by Scheuermann et al. agrees with one of our candidates for the $\nu_1(A_g)$ mode. Note that the frequency of this mode is slightly different in monazite-type $PbCrO_4$ (840 cm^{-1}), $SrCrO_4$ (868 cm^{-1}), and $LaCrO_4$ (830 cm^{-1}),[49] which implies that the mode frequency is slightly sensitive to a change of the nine-coordinated cation (Sr, Cr, and La). However, the frequency difference from one

DOI: 10.1021/acs.inorgchem.5b01135
Inorg. Chem. 2015, 54, 7524−7535

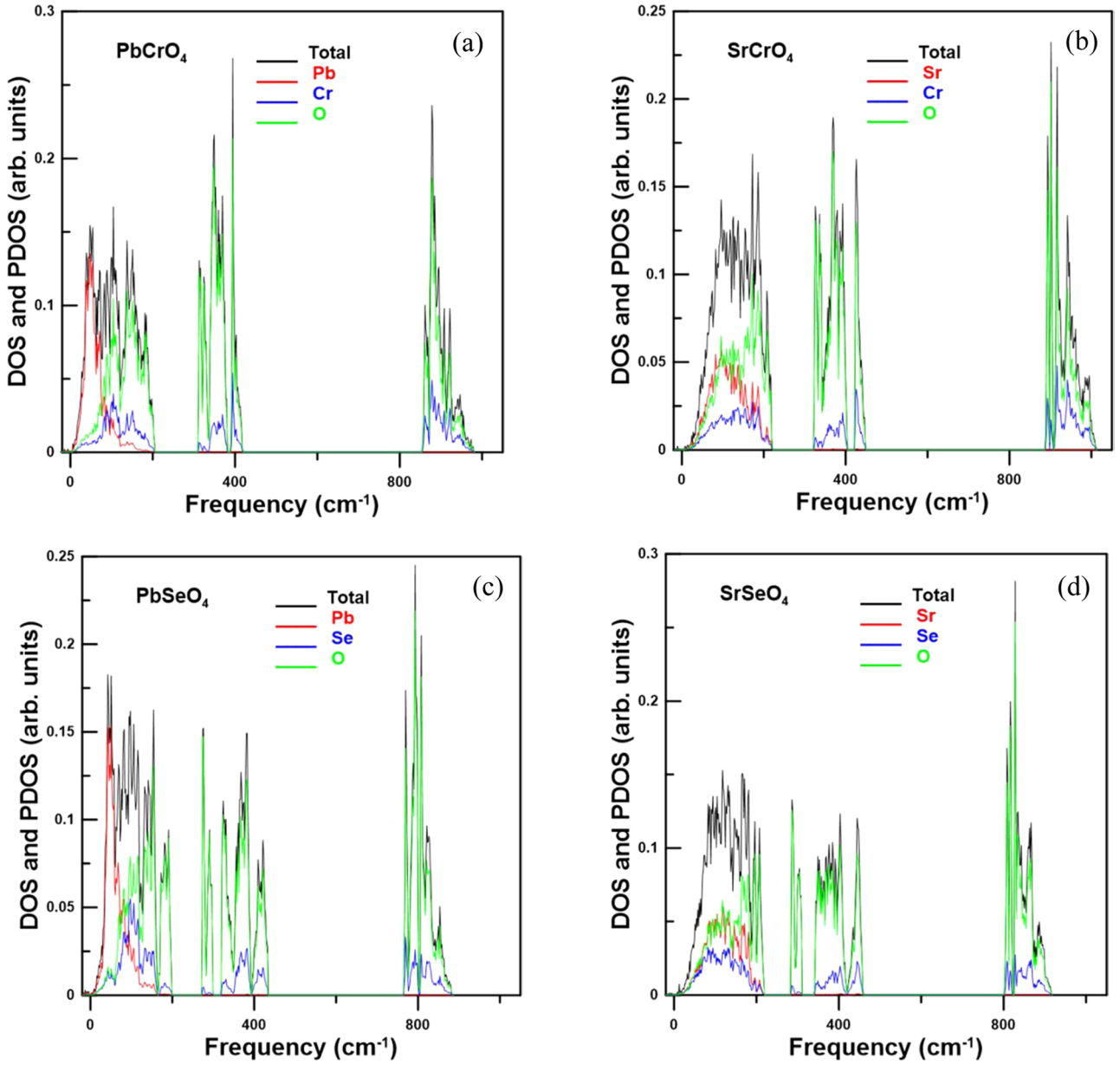

Figure 3. PDOSs of (a) $PbCrO_4$, (b) $SrCrO_4$, (c) $PbSeO_4$, and (d) $SrSeO_4$.

compound to the other is around 3%, while the frequency difference between the external modes of $SrCrO_4$ and $PbCrO_4$ range from 6% to 50%. These facts justify the use of the internal/external mode model as a first approximation to describe lattice vibrations in monazites.

It is also interesting to note here than in other chromates, where Cr is in tetrahedral coordination, that the symmetric stretching A_g mode is also always the most intense Raman-active mode, having frequencies similar to those observed in monazite-type chromates, e.g., $BaCrO_4$ (862 cm^{-1}),[50] $YCrO_4$ (863 cm^{-1}),[51] Ag_2CrO_4 (847 cm^{-1}),[52] $CaCrO_4$ (880 cm^{-1}),[53] and $NdCrO_4$ (844 cm^{-1}).[49] This fact is not a mere coincidence but a consequence of the fact that the mode frequency is basically determined by the Cr−O bond strength, which should be similar in all chromates discussed here because in all of them Cr is identically coordinated and the Cr−O distances are similar.[54] This is consistent with the fact that the frequency of the $\nu_1(A_g)$ mode decreases following the sequence $SrCrO_4$ (868 cm^{-1}) > $PbCrO_4$ (840 cm^{-1}) > $LaCrO_4$ (830 cm^{-1}) and the Cr−O average bond distance increases following the sequence $SrCrO_4$ (1.626 Å) > $PbCrO_4$ (1.663 Å) > $LaCrO_4$ (1.703 Å).

There are in the literature many empirical rules relating the Raman stretching frequencies to the bond length.[55] One of these is Badger's rule,[55] which has been found not to adequately correlate bond distances to stretching frequencies in chromates.[56] A more accurate relationship for chromates was developed by Weckhuysen and Wachs.[56] They proposed the following expression for the bond length−stretching frequency correlation:

$$\nu_1 = 13055 \exp(-1.6419R)$$

where ν_1 is in cm^{-1} and the Cr−O bond distance, R, in Å. Using this expression, we obtained ν_1 = 851 (886) cm^{-1} for $PbCrO_4$ ($SrCrO_4$). These values differ by less than 2% from the wavenumbers that we determined experimentally, which

DOI: 10.1021/acs.inorgchem.5b01135
Inorg. Chem. 2015, 54, 7524−7535

support the assignation that we made for the symmetric stretching mode.

To conclude the discussion on Raman modes, we would remark that, among the stretching modes, there should be 4 A_g and 4 B_g modes, which is in agreement with our mode assignment (see Table 4). In addition, among the bending modes, there should be 6 A_g and 6 B_g modes, which have been properly identified in Table 4. Finally, we assigned 9 A_g and 9 B_g external modes for each compound as expected.

From our DFT calculations, we have also determined the IR-active frequencies for the four studied compounds. To the best of our knowledge, the only previous study of IR modes was made by Scheuermann et al.[43,44] more than 40 years ago. In their works, between 4 and 10 modes were reported for the different compounds. They are summarized in Table 5. In the table, we also report the calculated frequencies for the 33 IR-active modes, together with their mode assignment. Again, the modes can be divided into external (13 modes), internal bending (10 modes), and internal stretching (8 modes). The three types of modes are separated by dotted lines in the table, going from external modes in the top (low-wavenumber region), to internal bending in the center (central-wavenumber region), and internal stretching in the bottom (high-wavenumber region). The IR mode distribution in frequencies is qualitatively similar to the Raman mode distribution. The information obtained from our calculations and summarized in Table 5 will allow mode assignment in future experiments. As can be seen in the table, the agreement between the calculated and measured IR modes is as good as that for the Raman modes. Therefore, our calculations can be a good guide in future IR measurements. Note that previous studies did not report any of the external IR modes.

To conclude the discussion of lattice vibrations, we would comment that, in addition to phonon frequencies at the Γ point, we have also calculated the PDOSs for the four compounds, which are given in Figure 3. As can be seen, in the harmonic approximation, there are no imaginary phonon branches near the Γ point; therefore, the monazite phase is dynamically stable. In general, the PDOSs of the four compounds present three zones separated by two phonon gaps: one around ≈200−300 cm^{-1} and another larger one between ≈400 and ≈800 cm^{-1}. According to the PDOS, it is observed that in the low-frequency zone the PDOS is composed of vibrations of PbO_9 (SrO_9) polyhedra and a lower contribution by CrO_4 (SeO_4) tetrahedra. The intermediate-frequency zone is mainly due to vibrations from the tetrahedron with a very small contribution from the PbO_9 (SrO_9) polyhedra, while the high-frequency zone is only due to vibrations from CrO_4 (SeO_4). In this sense, the vibrational spectra of the four studied compounds can be interpreted in terms of modes from the CrO_4 (SeO_4) tetrahedra, which can be considered as independent units in the monazite structure. Thus, our calculations confirm that the phonon modes in the studied monazites can be classified either as internal (the CrO_4 or SeO_4 center of mass does not move) or as external (movements of CrO_4 or SeO_4 tetrahedra as rigid units).

We will now describe the results of the optical-absorption studies. The absorption coefficient (α) of the four studied compounds at ambient conditions is shown in Figure 4 (top). The absorption spectrum shows a steep absorption, which corresponds to the fundamental absorption plus a low-energy absorption band that overlaps partially with the fundamental absorption. The low-energy absorption band has been

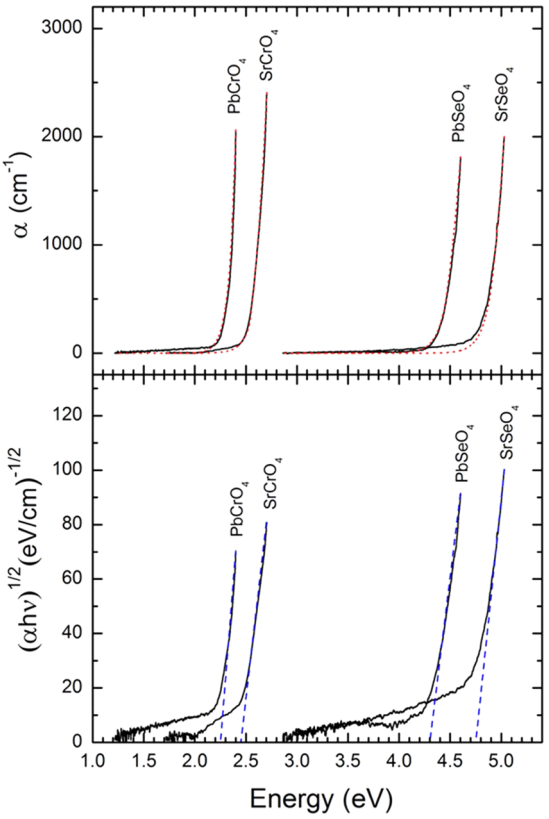

Figure 4. (Top) Measured absorption spectra (solid lines) and fits (dotted lines). (Bottom) Tauc plots used to determine E_g. The dashed lines show extrapolation of the linear region to the abscissa.

Table 6. Experimental and Theoretical Values of the Band Gaps (E_g) at Ambient Pressure

	experiment		theory	
compound	E_g (eV)	E_u (eV)	E_g (eV)	
$PbCrO_4$	2.25(5)	0.066(6)	A–Y → Y: 1.6183	Y → Y: 1.7153
$SrCrO_4$	2.45(5)	0.083(8)	Y → Z–Γ: 2.6762	Y → Γ: 2.6860
$PbSeO_4$	4.30(5)	0.090(9)	Y → C: 3.1798	C → C: 3.2832
$SrSeO_4$	4.75(5)	0.094(9)	Y → Γ: 3.6182	Γ → Γ: 3.6292

[a]The Urbach energy (E_u) determined from the fits to the experimental results is also included. For the calculations, we have listed the k points for the top of the valence band and bottom of the conduction band.

previously observed in related ternary oxides and seems to be related to the presence of defects.[17,26,27] Its nature has been the subject of considerable debate[57] and is beyond the scope of this work. This tail overlaps partially with the fundamental absorption, which makes it hard to conclude whether the smallest band gap is direct or indirect. In previous works, on the basis of the large values measured for the absorption coefficient of $PbCrO_4$, it was assumed that this material was a direct-band-gap material, determining that E_g was 2.3 eV.[6,17] However, the gradual increase of α (with respect to the photon energy) that we observed in the four studied compounds suggests an indirect nature for the fundamental band gap. Therefore, to determine more accurately the nature of the fundamental band gap, we analyzed the experimental results using a Tauc plot.[58] We found that for high energies $(\alpha h\nu)^{1/2}$ is proportional to the

DOI: 10.1021/acs.inorgchem.5b01135
Inorg. Chem. 2015, 54, 7524−7535

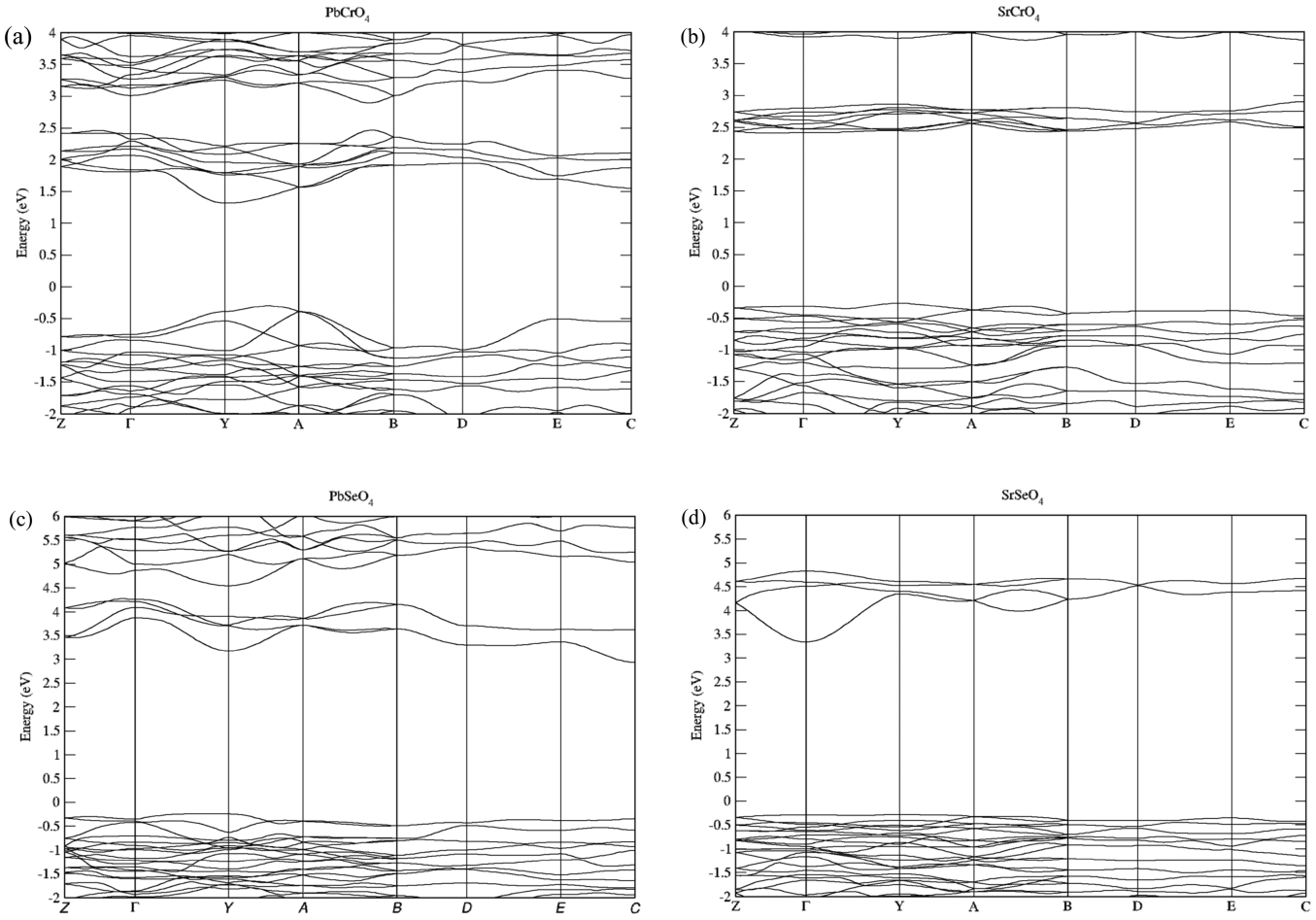

Figure 5. Band structures of (a) $PbCrO_4$, (b) $SrCrO_4$, (c) $PbSeO_4$, and (d) $SrSeO_4$.

photon energy ($h\nu$), as can be seen in Figure 4 (bottom), which supports the hypothesis that the four materials are indirect-band-gap semiconductors. This conclusion is in good agreement with our band-structure calculations. From the Tauc plots shown in Figure 4, we estimated E_g for the four compounds by extrapolating the linear region of $(\alpha h\nu)^{1/2}$ to the abscissa (blue dashed lines). The obtained values are summarized in Table 6. The value determined here for $PbCrO_4$ [E_g = 2.25(5) eV] is slightly smaller but consistent with the value that we determined previously (E_g = 2.3 eV). The band gap determined for $SrCrO_4$ [E_g = 2.45(5) eV] is consistent with the value determined by Yin et al. [E_g = 2.44(5) eV],[14] suggesting that other studies overestimate the value of E_g.[13−15]

In contrast with the chromates, which absorb visible light, we found that the selenates only absorb UV light and have band gaps more than 2 eV larger than those in their chromate counterpart. In addition, in Table 6, it can be seen that the Pb compounds have a smaller E_g than the Sr compounds, which is consistent with the observations when $PbWO_4$ ($PbMoO_4$) is compared with $SrWO_4$ ($SrMoO_4$).[59] The reasons for this behavior will be discussed when the results of the electronic structure calculations are described. Before going into this discussion, we would mention that the measured absorption spectra can be well fitted assuming that the low-energy part of the absorption edges exhibits an exponential dependence on the photon energy following Urbach's law[60] and that the high-energy part can be described by an allowed indirect transition. Under this assumption and when the phonon absorption and emission are neglected, the absorption spectrum is given by

$$\alpha(h\nu) = \begin{cases} A_1 e^{(h\nu - E_g)/E_u}, & h\nu \le E_g + 2E_u \\ A_2(h\nu - E_g)^2, & h\nu \ge E_g + 2E_u \end{cases}$$

where the parameters A_1 and A_2 are correlated by imposing that $\alpha(h\nu)$ should be continuously differentiable. This condition also determines the $E_g + 2E_u$ critical energy, below which the Urbach exponential absorption is assumed, where E_u is the Urbach energy. Assuming the E_g values determined from the Tauc plots (see Table 6) and using an iterative procedure, we have fitted the absorption spectra shown in Figure 4 (top). The fits (red dotted lines) reproduce well the experimental results (black solid lines), indicating that assuming an indirect band gap plus an Urbach tail is a reasonable hypothesis to describe the absorption spectra of the four studied compounds. From the fits, we have determined E_u, which is also related to the steepness of the absorption tail. The values obtained are summarized in Table 6. They are comparable with the values obtained in related ternary oxides.[17,26]

We will now discuss the results of the electronic structure calculations. The calculated band structures and DOSs of the four studied compounds are shown in Figures 5 and 6, respectively. The band structures are qualitatively similar in all cases. According to calculations, $PbCrO_4$, $PbSeO_4$, $SrCrO_4$, and $SrSeO_4$ are indirect-band-gap materials. This fact is in

DOI: 10.1021/acs.inorgchem.5b01135
Inorg. Chem. 2015, 54, 7524−7535

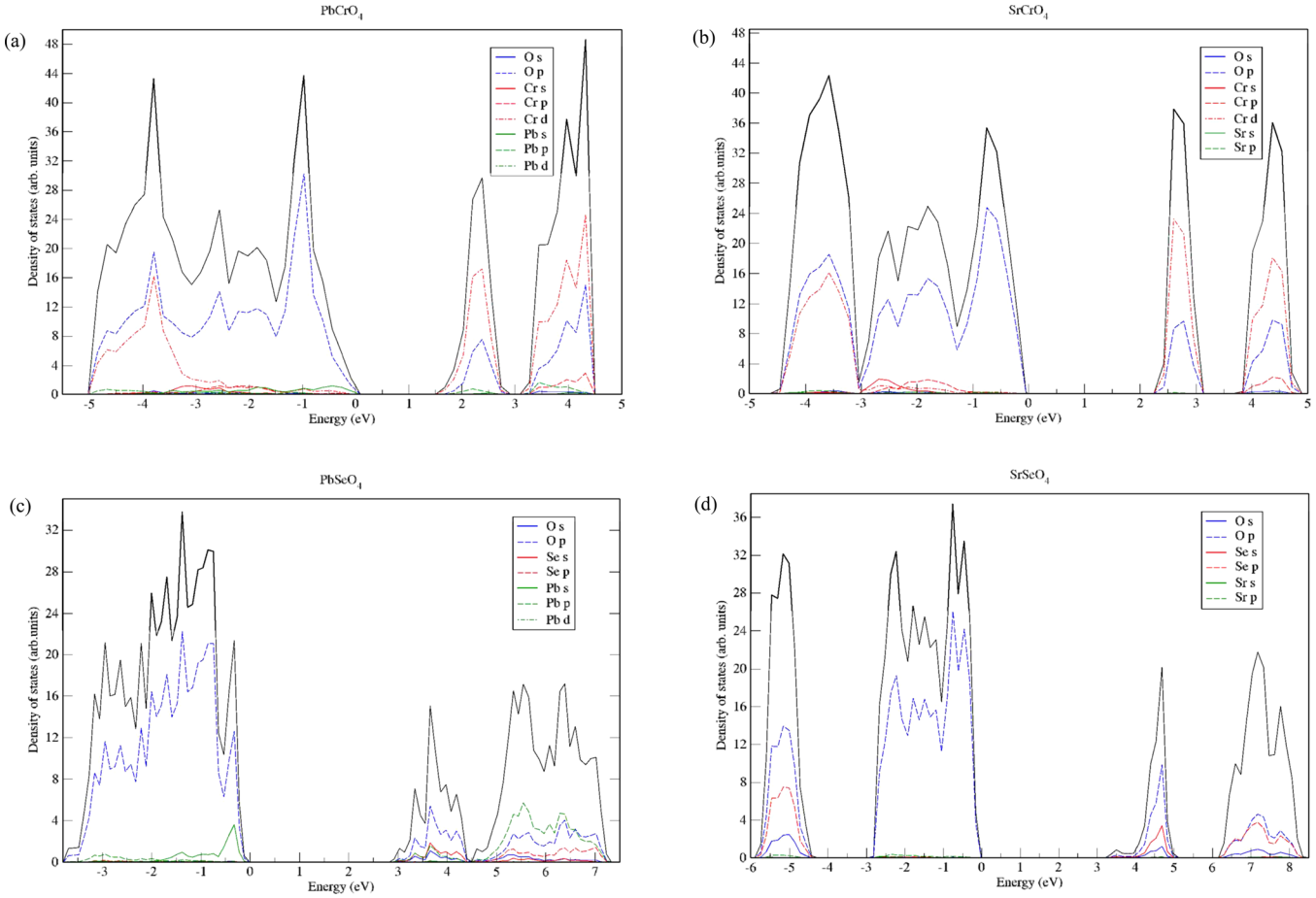

Figure 6. Total and partial DOSs of (a) $PbCrO_4$, (b) $SrCrO_4$, (c) $PbSeO_4$, and (d) $SrSeO_4$.

agreement with the conclusion extracted from the Tauc plot analysis. The calculated band-gap values are summarized in Table 6. These values underestimated the experimental values by around 1 eV (0.6 eV) in the selenates ($PbCrO_4$). In the case of $SrCrO_4$, theory slightly overestimates the band-gap energy (see Table 6). These discrepancies are typical of DFT calculations.[26,27] In spite of that, the calculated ordering of the band gaps is given by $PbCrO_4$ < $SrCrO_4$ < $PbSeO_4$ < $SrSeO_4$, which is in agreement with the experiments.

Let us describe now in detail the band structures of the different compounds (Figure 5). One important feature of the band structures is that, with the exception of $PbCrO_4$, the dispersion of the valence bands is relatively small, with comparable dispersions along different directions. In $PbCrO_4$, the maximum of the valence band is between the Y and A points of the BZ and the minimum of the conduction band at the Y point. Calculations also established that the Y−Y direct band gap is 0.1 eV higher than the indirect band gap. In $SrCrO_4$, the maximum of the valence band is the Y point of the BZ. On the other hand, the conduction band has two minima very close in energy, one at the Γ point of the BZ and the other between the Z and Γ points. Consequently, $SrCrO_4$ has two indirect band gaps that are separated by only 0.01 eV, as shown in Table 6. In $PbSeO_4$, there are two maxima in the valence band at the Y and C points of the BZ, separated by 0.1 eV. Additionally, the minimum of the conduction band is also at the C point of the BZ. Consequently, $PbSeO_4$ has an indirect band gap of 3.17 eV and a direct band gap of 3.28 eV. In the fourth compound, $SrSeO_4$, there are two maxima in the valence band separated by 0.01 eV, at the Y and Γ points of the BZ. In this material, the minimum of the conduction band is at the Γ point of the BZ. Consequently, $SrSeO_4$ has an indirect band gap and a direct band gap, which are nearly degenerated.

We will discuss now the nature and relative magnitude of the band gaps of the different studied compounds. In order to do this, we will use the calculated DOSs given in Figure 6. It can be seen that, in the four compounds, the upper part of the valence band is dominated by O 2p states. On the contrary, the lower part of the conduction band is composed primarily of electronic states associated with the Cr 3d (Se 4s) and O 2p states. Therefore, as a first approximation, it can be considered that the band-gap energy of the chromates and selenates is mainly determined by the molecular electronic structure of the CrO_4^{2-} and SeO_4^{2-} ions in which the hexavalent atom is in a tetrahedral environment. The classical field splitting in the SeO_4^{2-} ion is much larger than that in CrO_4^{2-} ion, which strongly supports our previous statement. Additional support to our conclusion comes from the fact that different related ternary oxides containing Pb (and having related crystal structures) have band gaps ordered following the sequence $PbCrO_4$ < $PbMoO_4$ < $PbWO_4$ < $PbSeO_4$. That is, the band gap increases as the field splitting increases: CrO_4^{2-} < MoO_4^{2-} < WO_4^{2-} < SeO_4^{2-}. Another important fact that can be seen in Figure 6 is that the Sr states are completely empty near the Fermi level. Thus, they do not have any influence on the band-gap energy. On the contrary, in $PbCrO_4$ and $PbSeO_4$, there is a contribution of Pb 6s electrons to the top of the valence band and of Pb 6p states to the bottom of the conduction band.

DOI: 10.1021/acs.inorgchem.5b01135
Inorg. Chem. 2015, 54, 7524−7535

As a consequence, the band gap is smaller in the Pb compounds than in the Sr compounds, as we found in the experiments. Notice that the same conclusion can be extracted from the comparison of the band gaps of $PbWO_4$ ($PbMoO_4$) and $SrWO_4$ ($SrMoO_4$).[59]

5. CONCLUDING REMARKS

We performed an experimental and theoretical study of $PbCrO_4$, $SrCrO_4$, $PbSeO_4$, and $SrSeO_4$ that has allowed us to analyze the structural, electronic, and vibrational properties of the four compounds. We found that calculations accurately reproduce the crystal structure of the four materials. They also are useful to deepen the understanding of the electronic and vibrational properties. In particular, calculations have helped us with the assignment of phonon modes and allowed us to predict where future experiments might find the as-yet-unobserved IR-active modes. Finally, the study of the electronic structure has demonstrated that the studied chromates and selenates behave as indirect-band-gap materials, with the chromates having a band gap in the visible and the selenates a band gap in the UV. Using theoretical calculations, we have been able to propose an explanation to this fact and also understand why the Pb compounds have a smaller band gap than the Sr counterparts.

AUTHOR INFORMATION

Corresponding Author

*E-mail: daniel.errandonea@uv.es.

Author Contributions

The manuscript was written through contributions of all authors. All authors have given approval to the final version of the manuscript.

Notes

The authors declare no competing financial interest.

ACKNOWLEDGMENTS

Research supported by the Spanish government MINECO under Grants MAT2013-46649-C4-1/3-P and MAT2012-38364-C03-02. We also acknowledge the computer time provide by the MALTA cluster and the Red Española de Supercomputación. D.E. would like to thank Julius Gleissner for fruitful discussions and valuable suggestions on the study of strontium chromate.

REFERENCES

(1) Lopez-Moreno, S.; Errandonea, D.; Rodriguez-Hernandez, P.; Muñoz, A. *Inorg. Chem.* **2015**, *54*, 1765−1777.
(2) Errandonea, D.; Kumar, R. S. *Mater. Res. Bull.* **2014**, *60*, 206−211.
(3) Vinogradova, N. S.; Shchapova, Y. V.; Votyakov, S. L.; Ryzhkov, M. V.; Ivanovskii, A. L. *J. Struct. Chem.* **2014**, *55*, 809−815.
(4) Rafiuddin, M. R.; Mueller, E.; Grosvenor, A. P. *J. Phys. Chem. C* **2014**, *118*, 18000−18009.
(5) Yakymchuk, C.; Brown, M. *J. Geol. Soc.* **2014**, *171*, 465−479.
(6) Errandonea, D.; Bandiello, E.; Segura, A.; Hamlin, J. J.; Maple, M. B.; Rodriguez-Hernandez, P.; Muñoz, A. *J. Alloys Compd.* **2014**, *587*, 14−20.
(7) Errandonea, D.; Popescu, C.; Achary, S. N.; Tyagi, A. K.; Bettinelli, M. *Mater. Res. Bull.* **2014**, *50*, 279−284.
(8) Huang, T.; Lee, J. S.; Kung, J.; Lin, C. M. *Solid State Commun.* **2010**, *150*, 1845−1850.
(9) Clavier, N.; Podor, R.; Dacheux, N. *J. Eur. Ceram. Soc.* **2011**, *31*, 941−976.
(10) Achary, S. N.; Errandonea, D.; Muñoz, A.; Rodriguez-Hernandez, P.; Manjon, F. J.; Krishna, P. S. R.; Patwe, S. J.; Grover, V.; Tyagi, A. K. *Dalton Trans.* **2013**, *42*, 14999−15015.
(11) Williams, M. L.; Jercinovic, M. J.; Hetherington, C. J. *Annu. Rev. Earth Planet. Sci.* **2007**, *35*, 137−175.
(12) Ermakova, O.; Lopez-Solano, J.; Minikayev, R.; Carlson, S.; Kaminska, A.; Glowacki, M.; Berkowski, M.; Mujica, A.; Muñoz, A.; Paszkowicz, W. *Acta Crystallogr., Sect. B: Struct. Sci., Cryst. Eng. Mater.* **2014**, *70*, 533−538.
(13) Stoltzfus. M. W. Structure−property relationships in solid state materials: A computational approach emphasizing chemical bonding. Ph.D. Thesis, The Ohio State University, Columbus, OH, 2007.
(14) Yin, J.; Zou, Z.; Ye, J. *Chem. Phys. Lett.* **2003**, *378*, 24−28.
(15) Parhi, P.; Manivannan, V. *J. Alloys Compd.* **2009**, *469*, 558−564.
(16) Gomez-Quero, S.; Hernandez-Mejia, C.; Hendrikx, R.; Rothenberg, G. *Dalton Trans.* **2012**, *41*, 12289−12295.
(17) Bandiello, E.; Errandonea, D.; Martinez-Garcia, D.; Santamaria-Perez, D.; Manjon, F. J. *Phys. Rev. B: Condens. Matter Mater. Phys.* **2012**, *85*, 024108.
(18) Miseki, Y.; Kitao, O.; Sayama, K. *RSC Adv.* **2015**, *5*, 1452−1455.
(19) Schenker, R. P.; Brunold, T. C.; Güdel, H. U. *Inorg. Chem.* **1998**, *37*, 918−927.
(20) Pistorius, C. W. F. T.; Pistorius, M. C. *Zeitschrift für Kristallographie* **1962**, *117*, 259−272.
(21) Effenberger, H.; Pertlik, F. *Zeitschrift fur Kristallographie* **1986**, *176*, 75−83.
(22) Wyckoff, R. W. G. *Structure of Crystals*; Interscience Publishers: New York, 1951; Vol. 3, pp 46−47.
(23) Knight, K. S. *Mineral. Mag.* **2000**, *64*, 291.
(24) Errandonea, D. *J. Appl. Phys.* **2010**, *108*, 033517.
(25) Segura, A.; Sans, J. A.; Errandonea, D.; Martinez-Garcia, D.; Fages, V. *Appl. Phys. Lett.* **2006**, *88*, 011910.
(26) Ruiz-Fuertes, J.; Lopez-Moreno, S.; Lopez-Solano, J.; Errandonea, D.; Segura, A.; Lacomba-Perales, R.; Muñoz, A.; Radescu, S.; Rodríguez-Hernández, P.; Gospodinov, M.; Nagornaya, L. L.; Tu, C. Y. *Phys. Rev. B: Condens. Matter Mater. Phys.* **2012**, *86*, 125202.
(27) Panchal, V.; Errandonea, D.; Segura, A.; Rodriguez-Hernandez, P.; Muñoz, A.; Lopez-Moreno, S.; Bettinelli, M. *J. Appl. Phys.* **2011**, *110*, 043723.
(28) Kresse, G.; Furthmuller, J. *Phys. Rev. B: Condens. Matter Mater. Phys.* **1996**, *54*, 11169−11186.
(29) Perdew, J. P.; Ruzsinszky, A.; Csonka, G. I.; Vydrov, O. A.; Scuseria, G. E.; Constantin, L. A.; Zhou, X.; Burke, K. *Phys. Rev. Lett.* **2008**, *100*, 136406.
(30) Hohenberg, P.; Kohn, W. *Phys. Rev.* **1964**, *136*, B864.
(31) Kresse, G.; Joubert, D. *Phys. Rev. B: Condens. Matter Mater. Phys.* **1999**, *59*, 1758−1775.
(32) Monkhorst, H. J.; Pack, J. D. *Phys. Rev. B* **1976**, *13*, 5188.
(33) Parlinski, K. Computer code PHONON, http://wolf.ifj.edu.pl/phonon/.
(34) Baroni, S.; de Gironcoli, S.; dal Corso, A.; Giannozzi, P. *Rev. Mod. Phys.* **2001**, *73*, 515.
(35) Mujica, A.; Rubio, A.; Muñoz, A.; Needs, R. J. *Rev. Mod. Phys.* **2003**, *75*, 863.
(36) Cazorla, C.; Íñiguez, J. *Phys. Rev. B: Condens. Matter Mater. Phys.* **2013**, *88*, 214430.
(37) Cazorla, C.; Boronat, J. *Phys. Rev. B: Condens. Matter Mater. Phys.* **2015**, *91*, 024103.
(38) Birch, F. *Phys. Rev.* **1947**, *71*, 809.
(39) Errandonea, D.; Santamaria-Perez, D.; Grover, V.; Achary, S. N.; Tyagi, A. K. *J. Appl. Phys.* **2010**, *108*, 073518.
(40) Errandonea, D.; Pellicer-Porres, J.; Manjón, F. J.; Segura, A.; Ferrer-Roca, Ch.; Kumar, R. S.; Tschauner, O.; López-Solano, J.; Rodríguez-Hernández, P.; Radescu, S.; Mujica, A.; Muñoz, A.; Aquilanti, G. *Phys. Rev. B: Condens. Matter Mater. Phys.* **2006**, *73*, 224103.
(41) Errandonea, D.; Kumar, R. S.; Ma, X.; Tu, C. *J. Solid State Chem.* **2008**, *181*, 355−364.

DOI: 10.1021/acs.inorgchem.5b01135
Inorg. Chem. 2015, 54, 7524−7535

(42) Errandonea, D.; Pellicer-Porres, J.; Manjón, F. J.; Segura, A.; Ferrer-Roca, Ch.; Kumar, R. S.; Tschauner, O.; López-Solano, J.; Rodríguez-Hernández, P.; Radescu, S.; Mujica, A.; Muñoz, A.; Aquilanti, G. *Phys. Rev. B: Condens. Matter Mater. Phys.* **2005**, *72*, 174106.
(43) Scheuermann, W.; Ritter, G. J.; Schutte, C. J. H. *Z. Naturforsch., A: Phys. Sci.* **1970**, *25*, 1856−1870.
(44) Scheuermann, W.; Schutte, C. J. H. *J. Raman Spectrosc.* **1973**, *1*, 619−627.
(45) Errandonea, D.; Gracia, L.; Lacomba-Perales, R.; Polian, A.; Chervin, J. C. *J. Appl. Phys.* **2013**, *113*, 123510.
(46) Gracia, L.; Beltrán, A.; Errandonea, D.; Andrés, J. *Inorg. Chem.* **2012**, *51*, 1751−1759.
(47) Ni, Y.; Hughes, J. M.; Mariano, N. *Am. Mineral.* **1995**, *80*, 21−26.
(48) Silva, E. N.; Ayala, A. P.; Guedes, I.; Paschoal, C. W. A.; Moreira, R. L.; Loong, C. K.; Boatner, L. A. *Opt. Mater.* **2006**, *29*, 224−230.
(49) Aoki, Y.; Konno, H.; Tachikawa, H.; Inagaki, M. *Bull. Chem. Soc. Jpn.* **2000**, *73*, 1197−1203.
(50) Huang, T.; Shieh, S. R.; Akhmetov, A.; Liu, X.; Lin, C. M.; Lee, J. S. *Phys. Rev. B* **2010**, *81*, 21411.
(51) Errandonea, D.; Kumar, R. S.; Lopez-Solano, J.; Rodríguez-Hernández, P.; Muñoz, A.; Rabie, M. G.; Saez Puche, R. *Phys. Rev. B: Condens. Matter Mater. Phys.* **2011**, *83*, 134109.
(52) Santamaría-Pérez, D.; Bandiello, E.; Errandonea, D.; Ruiz-Fuertes, J.; Gomis, O.; Sans, J. A.; Manjón, F. J.; Rodríguez-Hernández, P.; Muñoz, A. *J. Phys. Chem. C* **2013**, *117*, 12239−12248.
(53) Long, Y. W.; Zhang, W. W.; Yang, L. X.; Yu, Y.; Yu, R. C.; Ding, S.; Liu, Y. L.; Jin, C. Q. *Appl. Phys. Lett.* **2005**, *87*, 181901.
(54) Hardcastle, F. D.; Wachs, I. E. *J. Raman Spectrosc.* **1995**, *26*, 397−405.
(55) Cioslowski, J.; Liu, G.; Mosquera Castro, R. A. *Chem. Phys. Lett.* **2000**, *331*, 497−501.
(56) Weckhuysen, B. M.; Wachs, I. E. *J. Chem. Soc., Faraday Trans.* **1996**, *92*, 1969.
(57) Itoh, M.; Yokota, H.; Horimoto, M.; Fujita, M.; Usuki, Y. *Phys. Status Solidi B* **2002**, *231*, 595−600.
(58) Tauc, J. *Mater. Res. Bull.* **1968**, *3*, 37−46.
(59) Lacomba-Perales, R.; Ruiz-Fuertes, J.; Errandonea, D.; Martínez-García, D.; Segura, A. *EPL* **2008**, *83*, 37002.
(60) Urbach, F. *Phys. Rev.* **1953**, *92*, 1324.

DOI: 10.1021/acs.inorgchem.5b01135
Inorg. Chem. 2015, 54, 7524−7535